Desalination and Water Treatment
www.deswater.com
doi: 10.5004/dwt.2020.25725

192 (2020) 327–339
July

A facile synthesis of $BiVO_4$ with effective photocatalysis for refractory organic dyes

Ying Zhu[a], Jingpeng Tao[a,b], Yuelong Qin[a,c], Kun Liu[c], Hanbing Zhang[a,d,*], Zhangfa Tong[d], Binbin Yu[e]

[a]*College of Resources, Environment, and Materials, Guangxi University, Nanning 530004, China, Tel. +86–13077776827; emails: coldicezhang0771@163.com (H. Zhang), 1397619913@qq.com (Y. Zhu), 1187273937@qq.com (J. Tao), 362666493@qq.com (Y. Qin)*
[b]*Market Supervision and Administration Bureau of Guangnan County, Yunnan Province, Guangnan 663300, China*
[c]*Scientific Research Academy of Guangxi Environmental Protection, Nanning 530002, China, email: 1010534815@qq.com (K. Liu)*
[d]*Guangxi Key Laboratory of Petrochemical Resource Processing and Process Intensification Technology, School of Chemistry and Chemical Engineering, Guangxi University, Nanning 530004, China, email: zhftong@sina.com (Z. Tong)*
[e]*College of Environmental Science and Engineering, Yangzhou University, Yangzhou 225009, China, email: bbyu@yzu.edu.cn (B. Yu)*

Received 2 August 2019; Accepted 14 February 2020

ABSTRACT

$BiVO_4$ has good potential for the removal of refractory organic dyes from wastewater. To simplify the synthetic technology and further improve the photocatalytic activity of $BiVO_4$, an improved route of $BiVO_4$ was proposed via a fast microwave-assisted hydrothermal process using sodium carboxymethylcellulose. pH, microwave heating temperature, and calcination were revealed to be the key factors controlling the morphology of $BiVO_4$. Under pH 9, microwave heating at 120°C for 90 min, $BiVO_4$ ellipsoidal morphology with a smaller size (calcination at 400°C, 4 h) and $BiVO_4$ ellipsoidal morphology with a bigger size (without calcination) were successfully prepared and exhibited effective degradation for refractory Congo red and Alizarin red S in terms of rapid degradation rate, high degradation efficiency, and broad pH range. The enhanced photocatalytic activity of the as-prepared $BiVO_4$ was mainly attributed to the unique morphology, narrower band gap, and lower recombination ratio of photoinduced electron-hole pairs under the present preparation conditions. In summary, the study is valuable for optimizing the synthetic conditions of $BiVO_4$ and promoting its potential application in photocatalytic degradation for refractory organic pollutants.

Keywords: Microwave hydrothermal method; Sodium carboxymethylcellulose (CMC); $BiVO_4$; Microstructure; Photocatalysis

1. Introduction

Photocatalytic technology is recognized as a promising and practical approach for the disposal of wastewater containing refractory pollutants because of its high mineralization efficiency and short reaction time [1,2]. More importantly, photocatalysis can decompose hazardous organic dyes into less harmful matters. Among numerous photocatalysts, $BiVO_4$ has received extensive attention due to properties such as good visible light ability, narrow band gap (E_g = 2.4 eV), good stability, and low cost [3]. Commonly synthesized methods of $BiVO_4$ include the co-precipitation method, liquid phase combustion method, hydrothermal/solvent thermal method, and high-temperature solid-phase method [4–6]. Nevertheless, these methods usually have been constrained by some outstanding questions such as long reaction time, high reaction temperature, high pressure, or the use of toxic surfactants. Meanwhile, the poor photocatalytic performance and low adsorption capacity restricted the application of $BiVO_4$.

* Corresponding author.

In past decades, massive wastewater containing organic dyes was produced due to the development of many industries such as textiles, paper, and other coloring industries [7]. These dyes in wastewater are risky in accordance with their carcinogenic as well as mutagenic effect, which easily poses a threat to the aquatic ecosystem and human health. Meanwhile, it is limited to the few dyes as model pollutants for evaluating $BiVO_4$ photocatalytic degradation performance, such as methylene blue, methyl orange, and Rhodamine B [8–10]. Alizarin red S (ARS) and Congo red (CR) are the representative anionic dyes. Both ARS and CR are detrimental to health especially at elevated concentrations, causing irritation of the respiratory tracts, gastrointestinal tracts, and inducing some neurologic disorders [11–13]. To date, it is relatively insufficient for the reports on anion dyes ARS and CR degradation by $BiVO_4$ [14,15]. To solve the above problems, an in-depth study is essential and necessary.

To obtain the facile and moderate preparation technology of $BiVO_4$, microwave-assisted hydrothermal is one of the most concerned improvement methods. Microwave heating is effective to reduce the difficulty of the reaction process, including shortening preparation time, reducing reaction temperature, and accelerating the effective transfer of polar molecules rotation ability [16–18]. Meanwhile, morphological control is a feasible method to improve the photocatalytic performance of $BiVO_4$ [19,20]. Morphology has a crucial impact on the size and form of $BiVO_4$, which determines the photocatalytic active sites and thus enhances the photocatalytic activity of $BiVO_4$, pH, calcination time, and temperature have been proved to be vital for constructing the different morphologies of $BiVO_4$ [21–24]. It is because that pH affects the crystal plane and size for $BiVO_4$ during the preparation process and calcination determines the microstructure and purity of $BiVO_4$ [15,16]. Moreover, the photocatalytic activity of $BiVO_4$ can be strengthened by surfactants modification [25,26]. Among various surfactants, sodium carboxymethyl cellulose (CMC) is cheap, non-toxic, environmentally-friendly, and soluble. Being a surfactant-containing polyelectrolyte nature, CMC can form complexes with divalent metal ions and high transparency in the UV and visible spectral regions [27]. CMC can be rapidly eliminated from the catalyst because of its high water solubility [28]. According to these above-mentioned characteristics, CMC is a suitable stabilizer to adjust the morphologies and defects of nanomaterials [29]. Although many previous studies have been done to ameliorate the catalytic property of $BiVO_4$, there is a lack of studies on the integration of microwave heating, pH and calcination control, and CMC modification to simplify the preparation conditions and improve the photocatalytic performance of $BiVO_4$.

In this study, the morphology of $BiVO_4$ was controlled by changing the reaction parameters including pH, microwave heating, and calcination, and using CMC modification. Firstly, the effects of preparation conditions on the morphology and characteristics of $BiVO_4$ were systematically studied. Secondly, $BiVO_4$ under optimum preparation conditions exhibited good photocatalytic performance for ARS and CR under visible light. Thirdly, the reusability of $BiVO_4$ was also investigated. Finally, the underlying mechanism of ARS and CR photocatalytic degradation over $BiVO_4$ was also explained in detail.

2. Experimental details

2.1. Materials

All the reagents were of analytical grade and employed without further purification. Bismuth nitrate pentahydrate ($Bi(NO_3)_3{\cdot}5H_2O$) and ARS ($C_{14}H_7NaO_7S$) were obtained from Sinopharm Chemical Reagent Co. Ltd., (Shanghai, China). Ammonium metavanadate (NH_4VO_3), ammonia ($NH_3{\cdot}H_2O$), pentahydrate ethanol (C_2H_5OH), sodium hydroxide (NaOH) and CR ($C_{32}H_{22}N_6Na_2O_6S_2$) were supplied by Guanghua Technology Co. Ltd., (Guangdong, China). Nitric acid (HNO_3) was obtained from Kelon Chemical Reagent Factory (Chengdu, China). Sodium carboxymethylcellulose ($C_8H_{16}NaO_8$) was purchased from Xilong Chemical Co. Ltd., (Guangdong, China). Deionized water was used in all experiments.

2.2. Synthesis of $BiVO_4$

The synthesis of $BiVO_4$ was as follows: firstly, the solids of $Bi(NO_3)_3{\cdot}5H_2O$ (15 mmol) and NH_4VO_3 (15 mmol) were fully dissolved into HNO_3 solution (4.0 mol L^{-1}, 50 mL) and NaOH solution (2.0 mol L^{-1}, 50 mL), respectively. Secondly, the corresponding CMC water solution (0.37%, 25 mL) was added dropwise into each of the two solutions and mixed adequately. After mixing the above solutions, the initial pH was 4.2. Thirdly, the solution initial pH was adjusted to 5, 6, 9, and 10 by using 0.1 mol L^{-1} HCl or 2 mmol L^{-1} NH_4OH solutions (the previous study has confirmed that the degradation of CR and ARS by $BiVO_4$ prepared at pH 9 was higher than that of other $BiVO_4$ sample prepared at other pH values [30]. Therefore, $BiVO_4$ prepared at pH 9 was selected for follow-up study). Then, at optimum pH 9, the mixture was transferred into 100 mL Teflon autoclaves, heated in the microwave reactor (XH-800S, China) at 60°C, 120°C, and 200°C for 1.5 h (the previous study has confirmed that $BiVO_4$ prepared at 120°C exhibited better photocatalytic performance for CR and ARS than those prepared at temperature 60°C and 200°C [30]. Therefore, the sample prepared at pH 9, 120°C was selected for follow-up study). Subsequently, the obtained precipitate was washed with pure water and absolute ethanol. Thereafter, at optimum pH 9, 120°C, $BiVO_4$ without calcination was successfully obtained. Finally, under the same preparation conditions, the sample without calcination was calcined at 400°C for 4 h to obtain calcined $BiVO_4$. Therefore, each of the above factors was tested under the optimal level of the former factor. The schematic diagram for $BiVO_4$ synthesis is shown in Fig. 1.

2.3. Photocatalyst characterizations

The measurement conditions of X-ray diffraction (XRD, Rigaku, Japan) were set as follows: The working voltage and acceleration current of XRD were 40 kV and 20 mA respectively. The radiation source was Cu/Kα (λ = 0.154 nm and 2θ = 10°–80°) with a step size of 0.02° and a residence time of 0.5°/min. The XRD data was analyzed by Materials Data Jade 2010 analytical software. Fourier

transform infrared spectra were recorded on a Nicolet Nexus 470 apparatus with a KBr disk (Nicolet, America). The morphology of $BiVO_4$ was observed by field emission scanning electron microscopy (FE-SEM, Hitachi SU-8020, Japan). The $BiVO_4$ powder was dispersed in ethanol and mixed with ultrasound for 10 min. Then the mixture was dropped on the copper web and dried in natural air drying. Finally, $BiVO_4$ was moved into the vacuum chamber of FE-SEM for imaging. The UV-vis spectra of diffuse reflection (UV-vis DRS 3600, Shimadzu, Japan) of solid were recorded in the air at room temperature; Spectrometer was furnished with an integrating sphere accessory, and $BaSO_4$ was taken as background reference materials.

2.4. Photocatalytic activity testing of $BiVO_4$

To evaluate the photocatalytic activities of $BiVO_4$ samples, CR and ARS degradation were tested in the photochemical reaction (BL-GHX-II, China) with a 500 W Xe lamp illumination environments. According to our previous study, calcined $BiVO_4$ was more conducive to CR degradation than uncalcined $BiVO_4$, and uncalcined $BiVO_4$ was better than calcined $BiVO_4$ for ARS degradation [30]. Hence, in each experiment, calcined $BiVO_4$ (1.0 g L^{-1}, prepared at pH 9, 120°C) to CR solution (30 mg L^{-1}, 50 mL) and uncalcined $BiVO_4$ (1.0 g L^{-1}, prepared at pH 9, 120°C) to ARS (25 mg L^{-1}, 50 mL) solution were added to the quartz tubes. The quartz tubes circled the Xe light. Prior to the photocatalytic performance test, the suspension was ultrasonically dispersed in dark for 30 min for the purpose of reaching the adsorption–desorption equilibrium between dyes and $BiVO_4$. An aliquot (3 mL) was taken out from the reactor at certain time intervals during the illumination and then centrifuged at 6,000 rpm for 15 min. The corresponding concentration of ARS and CR at 518 and 494 nm were analyzed by UV-vis spectrophotometer (2550-Shimadzu, Japan), respectively. The degradation (%) of ARS and CR was evaluated by Eq. (1):

$$D_R = \left(1 - \frac{C_t}{C_0}\right) \times 100\% \quad (1)$$

where C_0 and C_t are the initial and at any time t concentrations of CR or ARS, respectively.

2.5. Recycling of $BiVO_4$

The reusability and stability were investigated by reusing the catalyst for the photocatalytic degradation experiments. The experimental process was the same as described in the experimental section. Between the two successive experiments, the catalysts were collected, filtered, dried, and reused in a new reaction to remove ARS and CR. Each cycle experiment was carried out with 1.0 g L^{-1} catalyst dosage 25 mg L^{-1} ARS and 30 mg L^{-1} CR under 3 h visible light irradiation. Moreover, the structural changes of $BiVO_4$ before and after 5 cycles were investigated by XRD, the characterization conditions were the same as before.

3. Results and discussion

3.1. Characterization of $BiVO_4$

Fig. 2a presents the XRD patterns of $BiVO_4$ at various pH values (pH 5, 6, 9, and 10). These diffraction peaks can be matched well with the monoclinic scheelite type $BiVO_4$ according to PDF standard card (JCPDS No. 14–0688). The characteristic peaks of $BiVO_4$ located at 19.6, 29.5, 31.1, 35.1°, 35.8°, 40.4°, 43.2°, 46.6°, 47.8°, 50.9°, 53.8°, 59.0°, and 59.8° (2θ) were in accordance with the (110), (121), (040), (200), (002), (211), (150), (060), (042), (222), (161), (321), and (123)

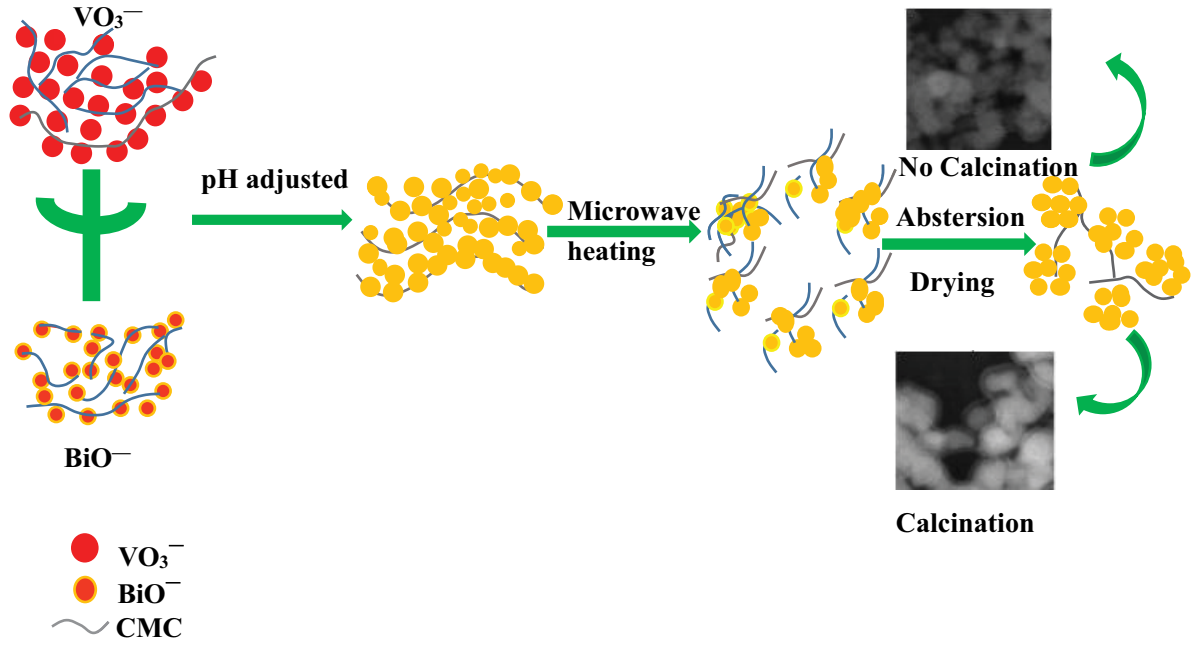

Fig. 1. Schematic diagram of the as-prepared $BiVO_4$.

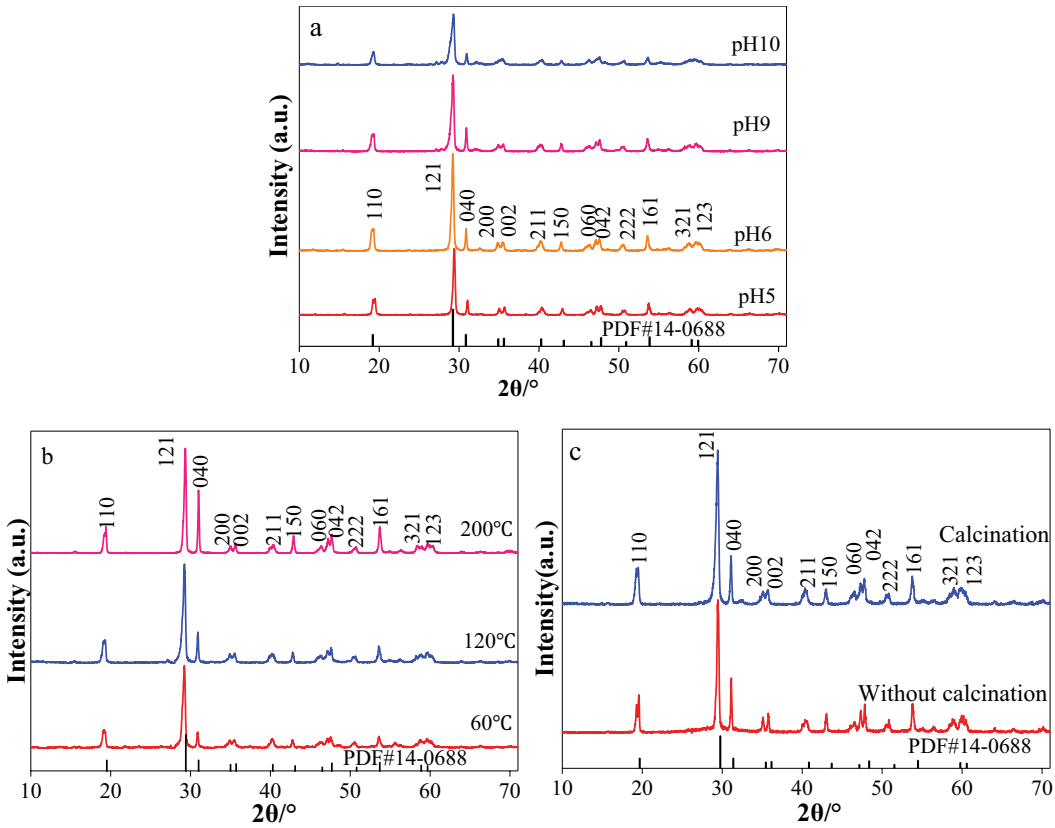

Fig. 2. XRD patterns of the $BiVO_4$ prepared under different conditions (a) pH: 5, 6, 9, and 10, (b) temperature: 60°C, 120°C, and 200°C, and (c) calcination and without calcination.

facets [8]. In addition, the diffraction peaks of all $BiVO_4$ samples were sharp and no other impurity peaks which indicated a good crystallinity of the samples [19]. The intensity of $BiVO_4$ diffraction peak prepared at pH 6 was the strongest, indicating that the crystallinity of $BiVO_4$ was the best under neutral conditions [31]. Fig. 2b indicates that all the diffraction peaks of $BiVO_4$ prepared at different temperatures were well-indexed to JCPDS No.14–0688, confirming the monoclinic scheelite type structure of the obtained $BiVO_4$ [10]. The half-peak width of $BiVO_4$ prepared at 120°C, 60°C, 200°C were 0.382, 0.372, and 0.292, respectively. The half-peak width of $BiVO_4$ prepared at 120°C was the largest, followed by 60°C and the smallest at 200°C, which illustrating that $BiVO_4$ size prepared at 200°C was the largest. The microwave hydrothermal temperature had a marked impact on the particle size of $BiVO_4$ [22]. XRD patterns of $BiVO_4$ prepared with calcination or without calcination in Fig. 2c suggests the characteristic peaks of the monoclinic scheelite type (JCPDS No.14–0688) in each sample. The ratio for (040)/(121) crystal facets diffraction peak was used to measure the exposure degree of (040) crystal facets [11]. The ratios for (040)/(121) with calcination or without calcination were 0.43 and 0.32, respectively, indicating that (040) crystal facets of the sample without calcination was higher. The intensity of the diffraction peak for $BiVO_4$ prepared at calcined was stronger and sharper than not calcined. This phenomenon demonstrated that calcination had a remarkable influence on the crystallinity and particle size of $BiVO_4$.

The FT-IR spectra of $BiVO_4$ prepared at pH 5, 6, 9, and 10 (Fig. 3a) were found wide infrared bands at 750–850 cm^{-1}, the symmetric and asymmetric stretching vibrations of V–O at 732 and 833 cm^{-1}, and bending vibration band of Bi–O at 678 cm^{-1} [32]. The characteristic stretching vibration functional groups –COO–, HO– and C–O–C of CMC were not found at 1,637; 1,408; 1,325; and 1,101 cm^{-1}, which implied that CMC was effectively removed after washing and calcination reaction [11]. The band at 1,386 cm^{-1} assigned to NO_3^- vibrations was found in $BiVO_4$ prepared at pH 6, 9, and 10, suggesting NO_3^- impurities were presented in $BiVO_4$ [32]. Nevertheless, there was no stretching vibration peak of NO_3^- was detected in $BiVO_4$ prepared at pH 5. CMC was the main cause of this phenomenon. CMC had the best viscosity within pH 6–10 and thus had a strong adsorption capacity for NO_3^-. Hence, NO_3^- cannot be removed by washing within pH 6–10. While CMC exhibited a poor viscosity of when solution pH lower than 5 and was easily hydrolyzed. Then CMC lost most of the colloidal property, which was beneficial for NO_3^- removal by washing because of the low adsorption capacity of CMC at pH 5.

Moreover, the FT-IR spectra of $BiVO_4$ prepared at 60°C, 120°C, and 200°C (Fig. 3b) were also found wide infrared bands at 550–850 cm^{-1}. The characteristic vibration bands of $BiVO_4$ at 730 and 798 cm^{-1} assigned to the stretching vibration bands of V–O, the bending vibration band of Bi–O at 647 cm^{-1} and the symmetric stretching vibration band of VO_4^{3-} at 472 cm^{-1} [19]. Additionally, the spectra also

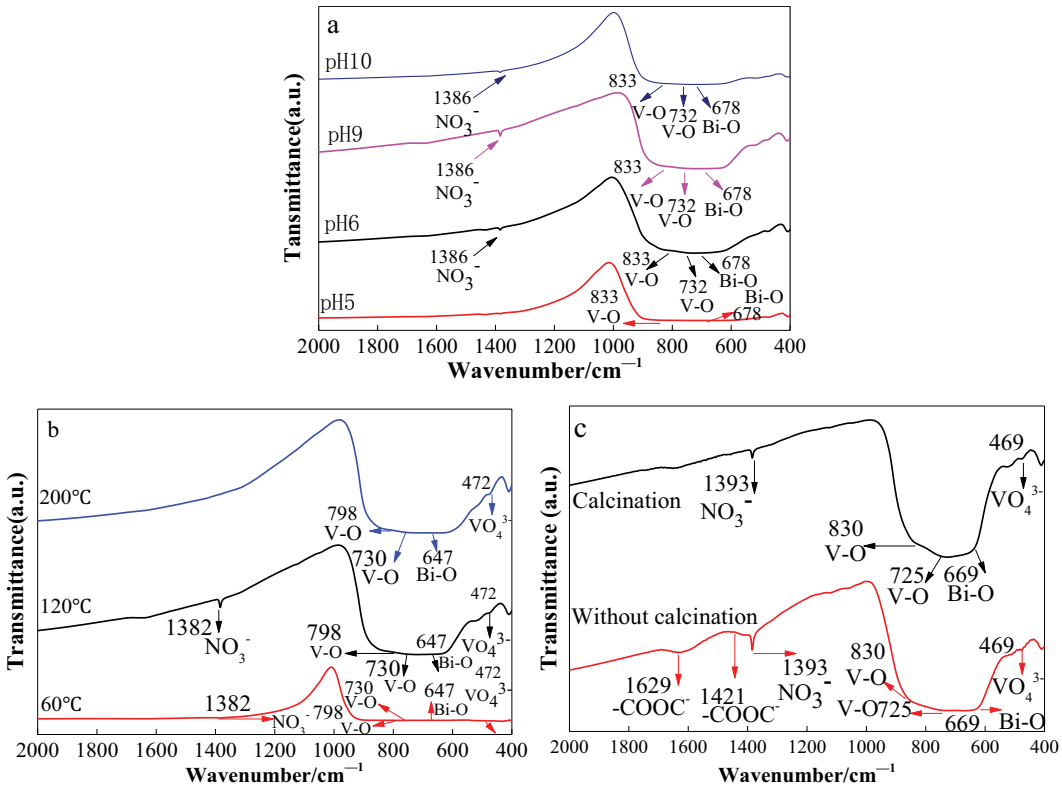

Fig. 3. FT-IR spectra of the $BiVO_4$ prepared under different conditions (a) pH: 5, 6, 9, and 10, (b) temperature: 60°C, 120°C, and 200°C, and (c) calcination and without calcination.

showed the bending vibration of NO_3^- at 1,390 cm^{-1} under $BiVO_4$ prepared at 60°C and 120°C [11]. The bending vibration of NO_3^- was not observed under $BiVO_4$ prepared at 200°C due to the carbonation of CMC caused NO_3^- to be re-released into the solutions. The characteristic stretching vibration functional groups of CMC were not found at 1,100–1,700 cm^{-1}, which implied that after washing and calcination reaction, CMC was effectively removed.

Fig. 3c exhibits the FT-IR spectra of $BiVO_4$ prepared under calcined and uncalcined conditions. A wide and high-intensity infrared band appeared in the vicinity of 736 cm^{-1} and the symmetric and asymmetric stretching vibrations of V–O at 725 and 830 cm^{-1} were observed of the samples [25]. The bending vibration band of Bi–O at 669 cm^{-1} and the symmetric stretching vibration band of VO_4^{3-} at 472 cm^{-1} were also observed of the samples [32]. The samples exhibited NO_3^- stretching vibration peaks at 1,393 cm^{-1} and the absorption peak intensity of the uncalcined sample was larger than that of the calcined sample. In addition, the characteristic stretching vibration functional groups –COOC– were found at 1,629 and 1,421 cm^{-1} in the uncalcined sample, which indicated that the purity of the uncalcined sample was low and CMC impurities were presented in the sample [33]. These results indicated that the structure and purity of $BiVO_4$ were affected by various pH values, heating temperature, and calcination.

The morphologies of $BiVO_4$ under different conditions were studied using FE–SEM analysis and the results are compiled in Fig. 4. Fig. 4a shows images of $BiVO_4$ prepared by microwave hydrothermal method with a surfactant under pH 5, 6, 9, and 10. There were obvious differences in morphologies of $BiVO_4$ powder depending on the pH values. At pH 5, $BiVO_4$ showed flakes with diameters of about 80–200 nm and particles with sizes of about 10–50 nm. The morphologies of $BiVO_4$ were different and the size dispersion was poor. At pH 6, $BiVO_4$ was composed of multiple particles to form an approximate T shape whose sizes were long side about 150 nm, short side about 70 nm, wide about 50 nm, and the dispersion was good. When pH value was 9, $BiVO_4$ had an elliptical morphology apparently with an average diameter of 60 nm in length. The samples were consistent in morphology and well dispersed in size. At pH 10, $BiVO_4$ had uniform size with an average diameter of 50 nm in length. $BiVO_4$ might be aggregated to some extent since there were many smaller particles on bigger ones. In addition, the size of $BiVO_4$ corresponding to pH 9 and 10 was smaller than that of pH 5 and 6, which were coincided with the results of XRD. It was indicated that pH had a remarkable effect on the morphologies development of $BiVO_4$.

Fig. 4b shows images of $BiVO_4$ prepared at microwave heating temperature 60°C, 120°C, and 200°C. $BiVO_4$ flakes with a size of 40–100 mm were obtained at 60°C. As the temperature further increased to 120°C, ellipsoid particles were generated with an average diameter of 60 nm in length. While the temperature was as high as 200°C, $BiVO_4$ exhibited a fishbone shaped structure with a length of about 8 μm and a width of about 4 μm. Evidently, $BiVO_4$ particles prepared at different temperatures exhibited

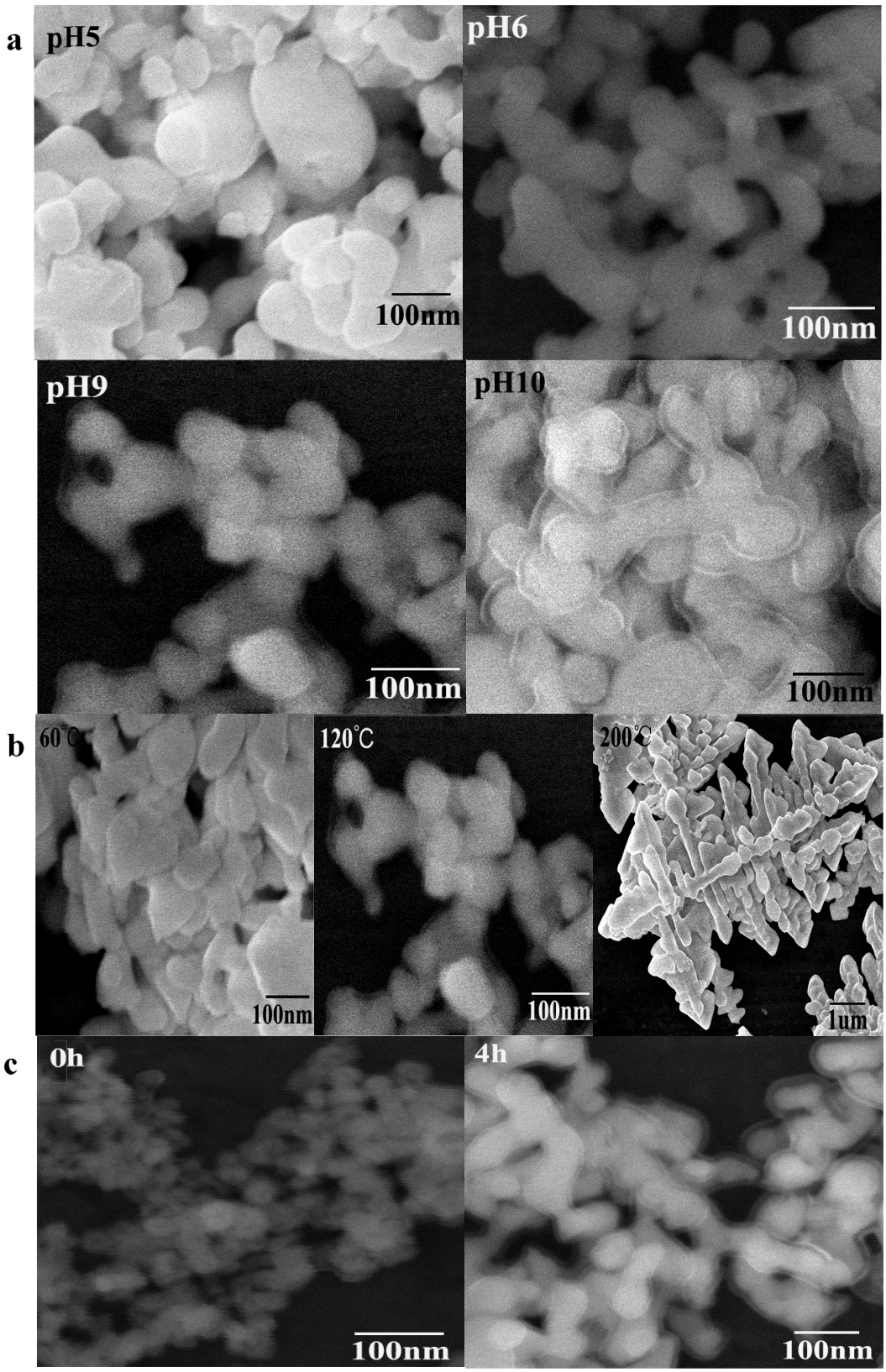

Fig. 4. FE-SEM images of the $BiVO_4$ prepared under different conditions (a) pH: 5, 6, 9, and 10, (b) temperature: 60°C, 120°C, and 200°C, (c) calcination and without calcination.

distinct morphology, which implied that heating temperature had a significant influence on the nucleation and growth behavior of the photocatalyst.

Fig. 4c shows images of $BiVO_4$ prepared with calcination and without calcination. $BiVO_4$ with an average particle size of about 30 nm which was not calcined had a plurality of particles joined together due to the high viscosity of CMC. A plurality of small particles was assembled into larger particles having an average particle diameter of about 50 nm due to CMC was mineralized after the sample was calcined. Compared with calcined $BiVO_4$, uncalcined $BiVO_4$ showed higher aggregation and poorer dispersibility. The results showed that calcination had an important influence on the particle size of $BiVO_4$.

The UV-vis absorption spectra of $BiVO_4$ are presented in Fig. 5. All the samples exhibited good absorption in the visible light region, which revealed the possibility of the photocatalytic response of these samples under visible light irradiation. Fig. 5a shows the UV-vis diffuse reflectance spectra of a series of $BiVO_4$ prepared at various pH values in the wavelength range of 300–800 nm. The band gap of $BiVO_4$ prepared at various pH values could be estimated by plotting Tauc's equation [34]. Thus, the band gaps were estimated to be 2.41, 2.40, 2.37, and 2.39 eV for $BiVO_4$ prepared at pH 5, 6, 9, and 10, respectively. It was apparent that the electronic structure of $BiVO_4$ varied with the changing of preparation pH values. In summary, UV–vis absorption spectra results indicated that pH played a key role in the visible light absorption capability of $BiVO_4$.

Fig. 5b shows UV-vis diffuse reflection spectra of $BiVO_4$ prepared at 60°C, 120°C, and 200°C. The band gaps were calculated to be 2.39, 2.37, and 2.41 eV for $BiVO_4$ prepared at 60°C, 120°C, and 200°C, respectively. The gaps of $BiVO_4$ were narrower, the particle size of $BiVO_4$ was smaller [3]. It was presumed that $BiVO_4$ prepared at 200°C had the largest size and $BiVO_4$ prepared at 120°C had the smallest size, which was in line with the FE-SEM and XRD characterization results. The band gaps were calculated to be 2.35 and 2.36 eV for $BiVO_4$ uncalcined and calcined (Fig. 5c). The band gap of uncalcined $BiVO_4$ was narrower than the band gap of calcined $BiVO_4$ due to its smaller particle size. Therefore, $BiVO_4$ prepared at pH 9, 120°C had better absorption ability under the visible light.

3.2. Comparison of $BiVO_4$ by different methods

The reported synthesis methods of $BiVO_4$ are compared with the current work in Table 1 [3–5,35–37]. Compared with the traditional methods of $BiVO_4$ synthesis, the role of microwave irradiation in current work can shorten the reaction time of $BiVO_4$, which proved again the benefits of microwave-assisted heating resulting in rapid reaction rate and good uniformity. In addition, CMC can be used as a good medium for absorbing and transferring microwave energy to the reactants, so it can promote the passage of energy barriers and accelerate the formation of $BiVO_4$ [27]. Therefore, the synthesis method introduced by CMC and microwave heating was more comparable than those listed

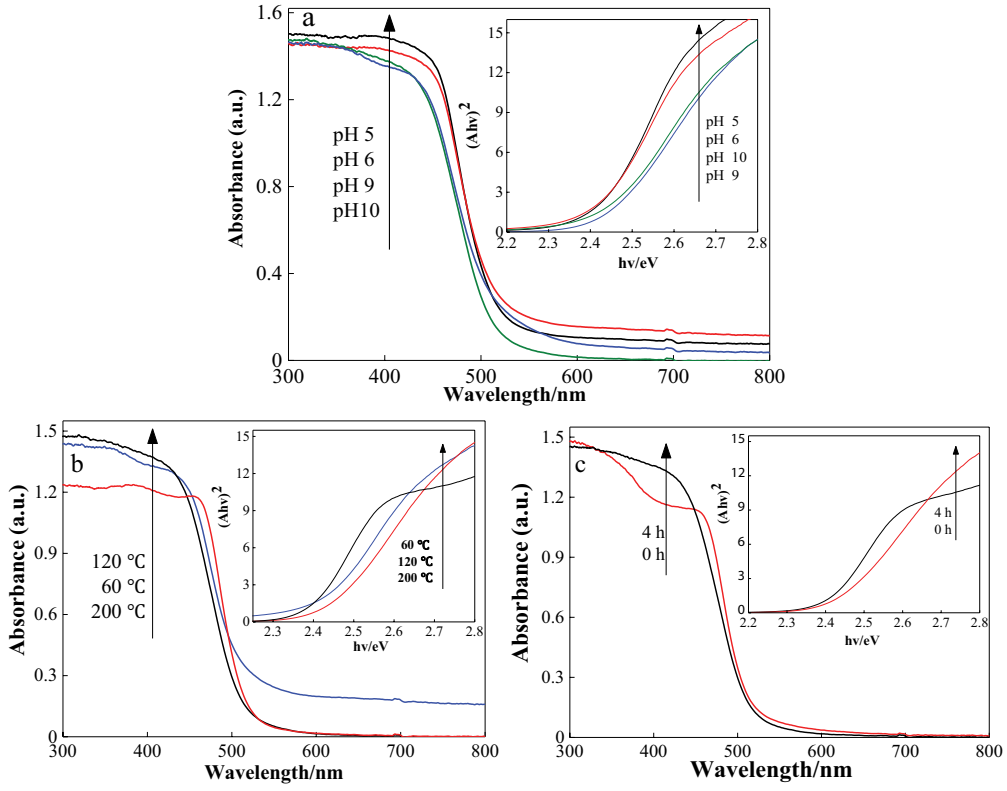

Fig. 5. UV-vis absorption spectra and $(Ahv)^2$–hv curves of the $BiVO_4$ under different conditions (a) pH: 5, 6, 9, and 10, (b) temperature: 60°C, 120°C, and 200°C, and (c) calcination and without calcination.

Table 1
Comparison of the $BiVO_4$ by different methods under various conditions

Method	Precursors	Reaction condition	Drying or calcination condition	Ref.
Hydrothermal method	$Bi(NO_3)_3{\cdot}5H_2O + NH_4VO_3 + C_{18}H_{33}NaO_2$	Stirred at room temperature for 2 h; 200°C, 12 h	Dried at 60°C for overnight	[4]
Solid-state reaction method	$Bi_2O_3 + V_2O_5$ + PVA	Ball-milled for 10 h; 600°C, 5 h	Calcined at 500°C for 13 h	[35]
Hydrothermal method	$Bi(NO_3)_3{\cdot}5H_2O + NH_4VO_3$	Stirred at room temperature for 1 h; 180°C, 24 h	Dried at 60°C for overnight	[3]
Solvothermal method	$BiCl_3 + Na_3VO_4$ + PVP	Stirred at room temperature for 1 h; 160°C, 5 h	Dried at 60°C for 12 h	[36]
Sol–gel method assisted by ultrasonication	$Bi(NO_3)_3{\cdot}5H_2O + NH_4VO_3$	Stirred at room temperature for 1 h; 70°C, 1.5 h	Dried at 100°C for 48 h; Calcined at 400°C for 2 h	[5]
Hydrothermal method	$Bi(NO_3)_3{\cdot}5H_2O + V_2O_5$	Stirred at room temperature for 48 h; 110°C, 10 h	Dried at 70°C for overnight	[37]
Microwave hydrothermal method	$Bi(NO_3)_3{\cdot}5H_2O + NH_4V_3 + HNO_3$ + CMC	Microwave radiation at 120°C for 1.5 h	Calcined at 400°C for 4 h	Current work
Microwave hydrothermal method	$Bi(NO_3)_3{\cdot}5H_2O + NH_4V_3 + HNO_3$ + CMC	Microwave radiation at 120°C for 1.5 h	No calcination	Current work

PVA, Polyvinyl alcohol; PVP, Polyvinyl pyrrolidone.

in other literature. The formed $BiVO_4$ was calcined at 400°C for 0 or 4 h to remove impurities (CMC), which was no obvious difference to the calcination conditions of other $BiVO_4$.

3.3. Photocatalytic activity

Two typical anionic dyes CR and ARS were selected as target contaminants to estimate the photocatalytic property of $BiVO_4$ under visible light. Fig. 6 shows the temporal variation of spectral changes of CR and ARS solutions during the degradation process under visible light by $BiVO_4$. The characteristic absorption peaks of both CR (~494 nm) and ARS (~518 nm) decreased with the prolongation of time. CR and ARS concentrations dramatically decreased because of the characteristic absorption peaks of CR and ARS at their respective maximum absorption wavelengths almost completely disappeared after 180 min of visible light irradiation. It was presumed that the active sites and groups were in contact with the dyes oxidation intermediates and mineralized, so the characteristic peaks of light absorption of dyes gradually disappeared from high to low [38]. On the basis of spectrum evolution, the absorption depletion occurred at the blue shift of absorption maximum. ARS shifted from 518 to 498 nm and the CR shifted from 494 to 475 nm, which may be the interference attributed to the desulfurization to generate new intermediates in the degradation process.

Fig. 7 depicts photolysis and photocatalytic degradation efficiency of CR and ARS vs. time interval plots. The photolysis efficiency of CR and ARS were almost non-existent, and the stability of CR and ARS were good during 3 h under visible light irradiation. However, $BiVO_4$ was able to bleach the CR ($BiVO_4$ with calcination) and ARS ($BiVO_4$ without calcination) solution 98% and 96% within 3 h under the same degradation reaction conditions. It was further confirmed the effective degradation of the two selected dyes by $BiVO_4$ again. In addition, based on the pseudo-first-order kinetic equation, the calculated kinetic rate constants of $BiVO_4$ were 0.022 min^{-1} for CR degradation and 0.017 min^{-1} for ARS degradation. Clearly, the photocatalytic degradation rate of CR was significantly faster than that of ARS.

The light absorption intensity of CR increased firstly and then decreased in the range of 200–700 nm with pH increase, while that of ARS always increased with pH increase (Fig. 8). Due to the fact that CR and ARS molecules existed in different forms at different pH values, thus exhibiting different colors and light absorption intensities [39]. The maximum absorption wavelength for CR decreased slightly with pH increase. The maximum absorption wavelength for ARS occurred with a redshift as pH increase.

Because $BiVO_4$ is a typical ternary oxide and has the characteristics of isoelectric point, the experiment about the effect of pH on the photodegradation of CR and ARS was conducted in the pH range of 4–11. Fig. 9 shows that the photocatalytic degradation efficiency of $BiVO_4$ was affected to some extent by variation in the initial pH of dyes solution. For CR, there was a gradual decrease from 98% to 80% in photocatalytic degradation efficiency with pH increase from 4 to 10. Acidic conditions were conducive to $BiVO_4$ degradation and the catalytic property of $BiVO_4$ was relatively stable under acidic conditions and near-neutral conditions. More positively charged surface sites of $BiVO_4$ became available thus facilitating greater CR anions adsorption under acidic conditions [40]. Under alkaline conditions, the catalysis was inhibited due to the change in electrostatic repulsion between CR and $BiVO_4$ [41]. Therefore, CR degradation decreased sharply to 63% at pH 11. For ARS, there

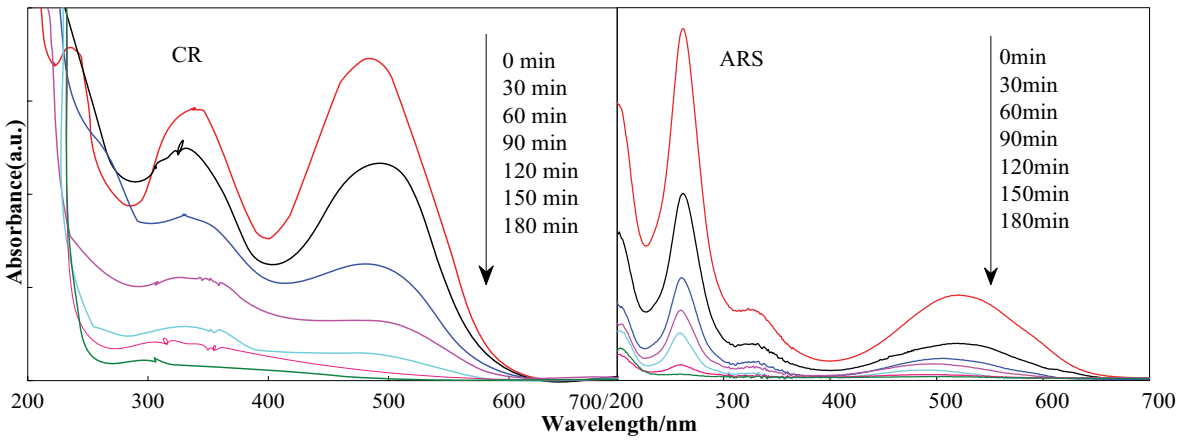

Fig. 6. UV–vis absorbance spectra of CR and ARS degradation by the $BiVO_4$.

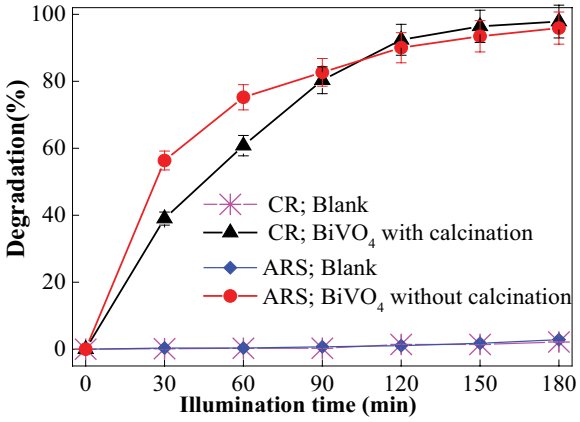

Fig. 7. Effect of illumination time on the photocatalytic degradation of CR and ARS.

was an increase in photocatalytic degradation with increasing pH from 4 to 7 and tended to be stable in pH from 7 to 11. Maximum ARS degradation (about 92%) by $BiVO_4$ without calcination was obtained at pH 9. It was indicated that $BiVO_4$ prepared under non-calcination conditions can exhibit good catalytic activity in neutral and alkaline environments. It was attributed to that the reaction between holes (h^+) in the valence band and OH groups produced a high concentration of free hydroxyl radicals to promote catalytic oxidation under alkaline conditions [14].

The photocatalytic properties of $BiVO_4$ for CR and ARS were compared with other various photocatalysts reported in the literature (Table 2) [42–49]. It can be seen that $BiVO_4$ has a relatively higher photocatalytic activity of refractory dyes in current work compared to other catalysts with the catalyst dosage and illumination time was not much different. The good photocatalytic performance of $BiVO_4$ could be related to the narrower band gap and smaller sizes [43,44].

3.4. Reusability of $BiVO_4$

The reusability and stability of $BiVO_4$ samples were investigated relative to 5 successive runs of CR and ARS degradation experiments. As presented in Fig. 10a, CR degradation by the calcined $BiVO_4$ decreased slightly in the 5 successive cycle runs, only about 0.4% decreased occurring in each run. Similarly, ARS degradation by the uncalcined $BiVO_4$ remained at approximately 90% after 5 successive cycles run indicating about 1.0 % decreased per each run. The highly stable and reusable properties of $BiVO_4$ samples could be of potential applications in environmental protection. The degradation performance of $BiVO_4$ might be attributed to the accumulation of catalytic degradation by-products on the surface of the catalyst in the preceding degradation cycle, which blocked the contact between dye molecules and catalyst particles and affected photon absorption [50]. Moreover, the slight loss of photocatalyst during the collection process and the inactivation of some active sites in the previous degradation cycle also led to $BiVO_4$ degradation performance decrease [51]. The structural and phase changes of $BiVO_4$ before and after 5 cycles of recycling were studied by XRD (Fig. 10b). It can be found that the crystal phases in the calcined or uncalcined $BiVO_4$ remained unchanged after 5 consecutive runs, indicating that the photocatalytic corrosion effect and oxidation of $BiVO_4$ rarely occurred. Overall, the as-prepared $BiVO_4$ not only had good recycling performance and catalytic activity but also had remained high catalytic stability during the process of multiple usages.

3.5. Photocatalytic mechanism

The photocatalytic mechanism of CR and ARS in the presence of $BiVO_4$ was proposed and the applicable reactions were shown as follows:

$$BiVO_4 + \text{visible light} \rightarrow BiVO_4\left(e^-_{CB} + h^+_{VB}\right) \quad (2)$$

$$BiVO_4\left(h^+_{VB}\right) + H_2O \rightarrow BiVO_4 + {}^{\bullet}OH + H^+ \quad (3)$$

$$BiVO_4\left(e^-_{CB}\right) + O_2 \rightarrow BiVO_4 + {}^{\bullet}O_2^- \quad (4)$$

$$BiVO_4\left(h^+_{VB}\right) + OH^- \rightarrow BiVO_4 + {}^{\bullet}OH \quad (5)$$

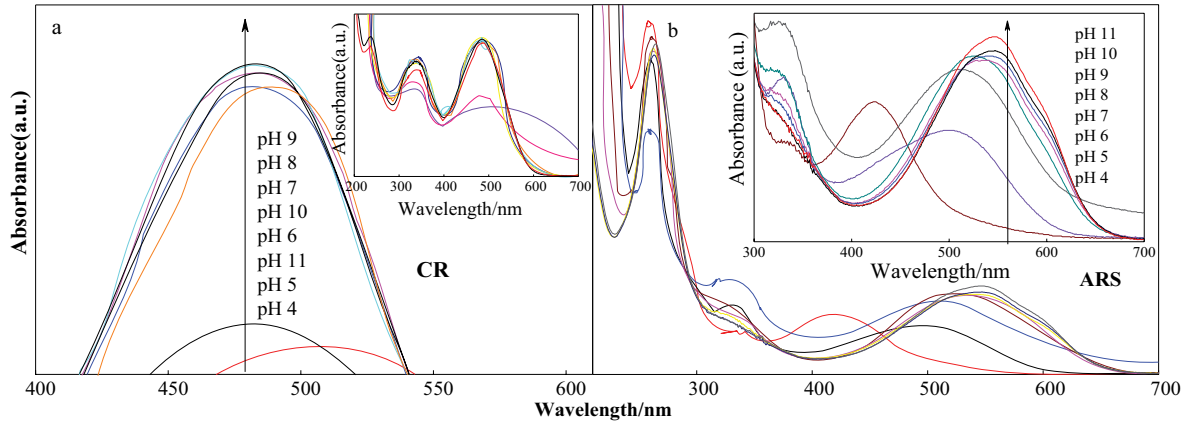

Fig. 8. UV-vis absorbance spectra of (a) CR and (b) ARS degradation at different pH values by the $BiVO_4$.

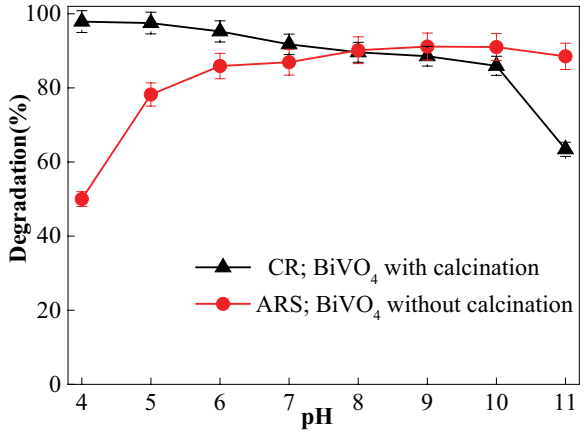

Fig. 9. Effect of initial pH on the photocatalytic degradation of CR and ARS.

$$^{\bullet}O_2^- + \text{CR / ARS} \rightarrow \text{degradation products} \quad (6)$$

$$^{\bullet}OH + \text{CR / ARS} \rightarrow \text{degradation products} \quad (7)$$

In line with reactions (2)–(7), the reasonable mechanism was also explained in Fig. 11. When $BiVO_4$ was subjected to visible light irradiation, the photogenerated electrons (e^-) could migrate from valance band (VB) to conduction band (CB), generating holes (h^+) in VB (Eq. (2)) [47]. The photogenerated holes would react with absorbed water on $BiVO_4$ surface to generate highly reactive hydroxyl radical ($^{\bullet}OH$), whereas O_2 acted as an electron acceptor to form a superoxide anion radical ($^{\bullet}O_2^-$) (Eqs. (3)–(5)) [14]. In addition, the photogenerated holes could be trapped by –OH thus preventing the recombination of electron-hole pairs [52]. Further, $^{\bullet}O_2^-$ can act as an oxidizer and remove CR and ARS (Eqs. (6)–(7)).

4. Conclusions

$BiVO_4$ was successfully synthesized via a fast microwave hydrothermal method assisted with CMC. The microwave hydrothermal method effectively reduced the temperature and time required to generate $BiVO_4$. Microwave heating temperature, pH, and calcination played important roles in changing the phases and morphologies of $BiVO_4$ for optimization. The as-obtained $BiVO_4$ demonstrated

Table 2
Comparison of the photocatalytic performance of various photocatalysts for CR and ARS degradation

Dyes	Photocatalyst	Light source	Photocatalytic time (h)	Catalyst dosage (g L^{-1})	Initial concentration (mg L^{-1})	Degradation (%)	Ref.
CR	WO_3	UV 6 W	5.0	1.7	10	74	[42]
CR	ZnO	UV 15 W	2.0	0.5	10	50	[43]
CR	P25 (TiO_2)	Visible light	3.5	1.0	30	90	[44]
CR	$Ni_{0.2}Cu_{0.8}Al_2O_4$	solar light	3.0	1.0	30	90	[45]
CR	$BiVO_4$	Visible light	3.0	1.0	30	98	Current work
ARS	ZnO	UV 18 W	2.0	1.0	25	77	[46]
ARS	Bi_2O_3:Ce^{3+}/Ce^{4+}	Visible light	2.5	1.0	20	90	[47]
ARS	P25 (TiO_2)	Visible light	3.0	0.5	20	80	[48]
ARS	MWCNTs + H_2O_2	UV 16 W	2.5	0.15	20	95	[49]
ARS	$BiVO_4$	Visible light	3.0	1.0	25	96	Current work

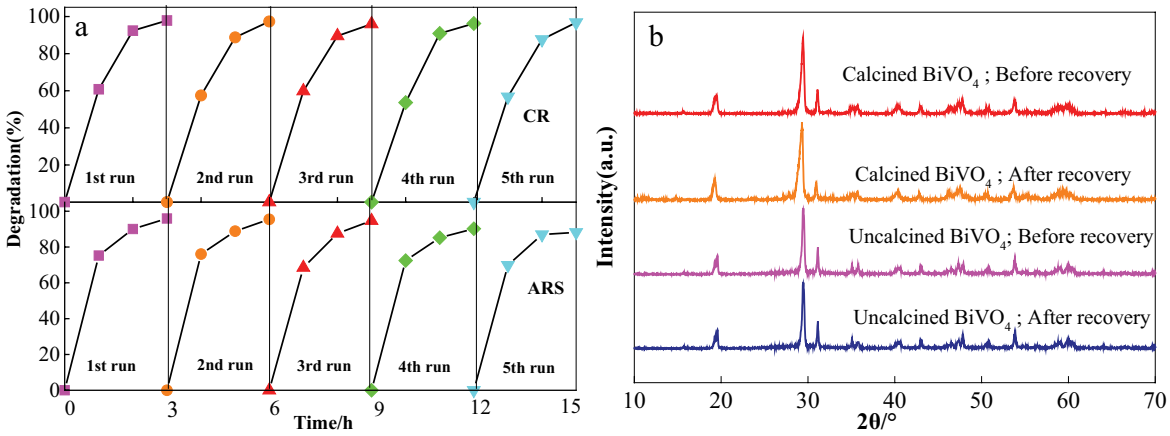

Fig. 10. (a) CR and ARS degradation by $BiVO_4$ during 5 successive runs and (b) XRD patterns of the $BiVO_4$ before and after 5 successive runs.

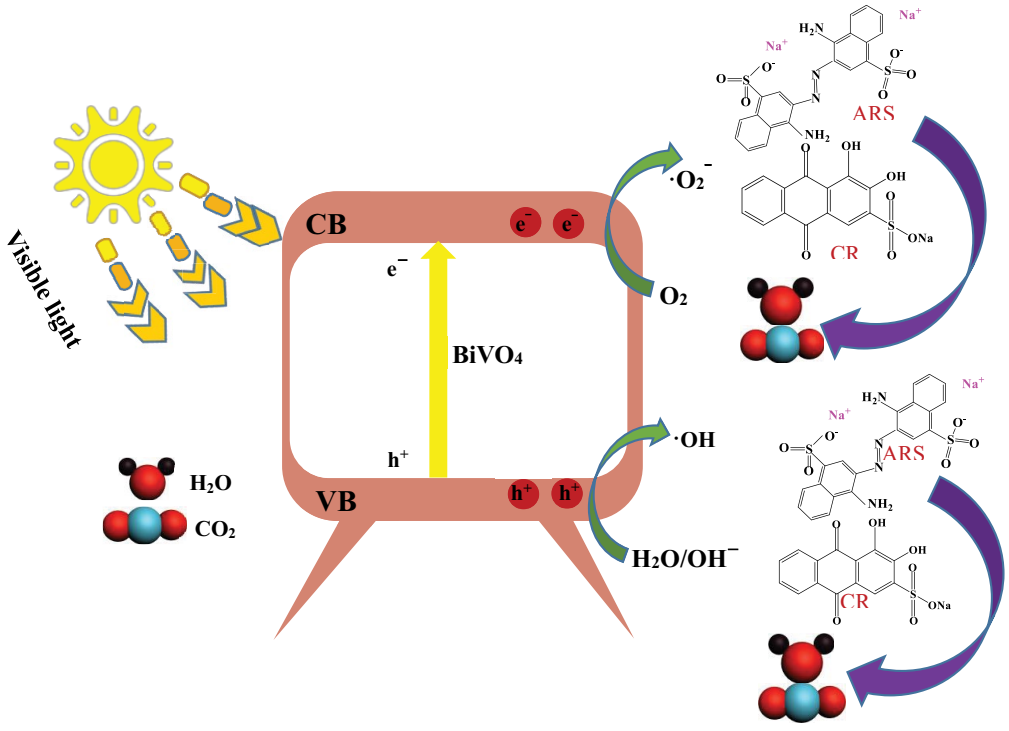

Fig. 11. Possible photocatalytic mechanism of CR and ARS by the $BiVO_4$ under visible light irradiation.

degradation for CR (98%) and ARS (96%) owing to elliptical morphology, strengthened separation ability of photoinduced electron-hole pairs. In addition, $BiVO_4$ exhibited good stability and recyclability after 5 cycles of degradation for CR and ARS. In all, this study will provide a feasible method to optimize the preparation and improve the photocatalytic activity of photocatalysts.

Acknowledgments

The authors gratefully acknowledge the financial support from the National Science Foundation of China (21576055, 31500425), the Jiangsu Provincial Natural Science Foundation of China (BK 20150452), and the Petrochemical Resources Processing and Process Reinforcement Technology Key Laboratory Project of Guangxi province (No. 2018Z004).

References

[1] W. Teng, Y. Wang, Q. Lin, H. Zhu, Y. Tang, X. Li, Synthesis of MoS_2/TiO_2 nanophotocatalyst and its enhanced visible light-driven photocatalytic performance, J. Nanosci. Nanotechnol., 19 (2019) 3519–3527.

[2] K. Sirirekratana, P. Kemacheevakul, S. Chuangchote, Color removal from wastewater by photocatalytic process using titanium dioxide-coated glass, ceramic tile, and stainless steel sheets, J. Cleaner Prod., 215 (2019) 123–130.

[3] Y. Lin, C. Lu, C. Wei, Microstructure and photocatalytic performance of $BiVO_4$ prepared by hydrothermal method, J. Alloys Compd., 781 (2019) 56–63.
[4] J. Xu, Z. Bian, X. Xin, A. Chen, H. Wang, Size dependence of nanosheet $BiVO_4$ with oxygen vacancies and exposed {0 0 1} facets on the photodegradation of oxytetracycline, Chem. Eng. J., 337 (2018) 684–696.
[5] J.P. Deebasree, V. Maheskumar, B. Vidhya, Investigation of the visible light photocatalytic activity of $BiVO_4$ prepared by sol–gel method assisted by ultrasonication, Ultrason. Sonochem., 45 (2018) 123–132.
[6] X. Zhang, Y. Huang, F. Ma, Z. Zhang, X. Wei, Influences of vacancies on the structural, electronic, and optical properties of monoclinic $BiVO_4$, J. Phys. Chem. Solids, 121 (2018) 85–92.
[7] G. Li, B. Wang, Q. Sun, W. Xu, Y. Han, Visible-light photocatalytic activity of Fe and/or Ni-doped ilmenite derived-titanium dioxide nanoparticles, J. Nanosci. Nanotechnol., 19 (2019) 3343–3355.
[8] H. Lee, S. Park, One-pot synthesis of reduced graphene oxide/anatase titanium dioxide composites for photocatalytic degradation of Methylene blue, J. Nanosci. Nanotechnol., 18 (2018) 6173–6179.
[9] L. Liu, R. Shan, Y. Shi, S. Wang, H. Yuan, A novel TiO_2/biochar composite catalysts for photocatalytic degradation of Methyl orange, Chemosphere, 222 (2019) 391–398.
[10] P.V. Gayathri, S. Yesodharan, E.P. Yesodharan, Purification of water contaminated with traces of Rhodamine B dye by microwave-assisted, oxidant-induced, and zinc oxide catalyzed advanced oxidation process, Desal. Water Treat., 85 (2017) 161–174.
[11] A. Burakw, E. Neskoromnaya, A. Babkin, Removal of the Alizarin red S anionic dye using graphene nanocomposites: a study on kinetics under dynamic conditions, Mater. Today, 11 (2019) 392–397.
[12] A. Jagusiak, T. Panczyk, Interaction of Congo red, Evans blue and Titan yellow with doxorubicin in aqueous solutions. A molecular dynamics study, J. Mol. Liq., 279 (2019) 640–648.
[13] H. Zhang, J. Zhou, Y. Muhammad, R. Tang, K. Liu, Y. Zhu, Z. Tong, Citric acid modified bentonite for Congo red adsorption, Front. Mater., 6 (2019) 1–11.
[14] C. Vicas, K. Namratha, M.B. Nayan, K. Byrappa, Controlled hydrothermal synthesis of bismuth vanadate nano-articulate structures: photooxidation of methicillin-resistant staphylococcus aureus and organic dyes, Mater. Today, 9 (2019) 468–480.
[15] M. Sajid, N. Amin, N. Shad, S. Kham, Y. Javed, Z. Zhang, Hydrothermal fabrication of monoclinic bismuth vanadate (m-$BiVO_4$) nanoparticles for photocatalytic degradation of toxic organic dyes, Mater. Sci. Eng., B, 242 (2019) 83–89.
[16] M. Xu, S. Jia, C. Chen, Z. Zhang, J. Yan, Y. Guo, Y. Zhang, W. Zhao, J. Yun, Y. Wang, Microwave-assistant hydrothermal synthesis of SnO_2@ZnO hierarchical nanostructures enhanced photocatalytic performance under visible light irradiation, Mater. Res. Bull., 106 (2018) 74–80.
[17] K. Liu, Y. Qin, Y. Muhammad, Y. Zhu, R. Tang, H. Zhang, Z. Tong, Effect of Fe_3O_4 content, and microwave reaction time on the properties of Fe_3O_4/ZnO magnetic nanoparticles, J. Alloys Compd., 781 (2019) 790–799.
[18] H. Zhang, Z. Song, D. Wang, Z. Tong, Y. Qin, A facile synthetic method of ZnO nanoparticles and its role in photocatalytic degradation of refractory organic matters, Desal. Water Treat., 90 (2017) 189–195.
[19] M. Sun, P. Guo, M. Wang, F. Ren, The effect of pH on the photocatalytic performance of $BiVO_4$ for phenol mine sewage degradation under visible light, Optik, 179 (2019) 672–679.
[20] Y. Lu, H. Shang, F. Shi, C. Chao, X. Zhang, B. Zhang, Preparation, and efficient visible-light-induced photocatalytic activity of m-$BiVO_4$ with different morphologies, J. Phys. Chem. Solids, 85 (2015) 44–50.
[21] M. Kim, E. Samuel, K. Kim, H. Yoon, B. Joshi, M. Swihart, S. Yoon, Tuning the morphology of electrosprayed $BiVO_4$ from nanopillars to nanoferns via pH control for solar water splitting, J. Alloys Compd., 789 (2018) 193–200.
[22] X. Li, L. Xu, K. Li, M. Hu, R. Huang, C. Huang, Oxidant peroxo-synthesized monoclinic $BiVO_4$: insights into the crystal structure deformation and the thermochromic properties, J. Alloys Compd., 787 (2019) 666–671.
[23] M. Wu, Q. Jing, X. Feng, L. Chen, $BiVO_4$ microstructures with various morphologies: synthesis and characterization, Appl. Surf. Sci., 427 (2018) 525–532.
[24] J. Luo, P. Fu, Y. Qu, Z. Lin, W. Zeng, The *n*-butanol gas-sensing properties of monoclinic scheelite $BiVO_4$ nanoplates, Physica E, 103 (2018) 71–75.
[25] Y. Lu, H. Shang, H. Guan, Y. Zhao, H. Zhang, B. Zhang, Enhanced visible-light photocatalytic activity of $BiVO_4$ microstructures via annealing process, Superlattices Microstruct., 88 (2015) 591–599.
[26] S. Zhao, H. Zuo, Y. Guo, Q. Pan, Carbon-doped ZnO aided by carboxymethyl cellulose: fabrication, photoluminescence, and photocatalytic applications, J. Alloys Compd., 695 (2017) 1029–1037.
[27] R.A. Ocampo, F.E. Echeverria, Effect of the anodization parameters on TiO_2 nanotubes characteristics produced in aqueous electrolytes with CMC, Appl. Surf. Sci., 469 (2019) 994–1006.
[28] A. Salama, S. Etri, S.A. Mohamed, M. Osakhawy, Carboxymethyl cellulose prepared from mesquite tree: new source for promising nanocomposite materials, Carbohydr. Polym., 189 (2018) 138–144.
[29] S. Javanbakht, M. Pwresmaeil, H. Namazi, Green one-pot synthesis of carboxymethylcellulose/Zn-based metal-organic framework/graphene oxide bio-nanocomposite as a nanocarrier for drug delivery system, Carbohydr. Polym., 208 (2019) 294–301.
[30] J.P. Tao, H.B. Zhang, Y.L. Qin, Z.Y. Song, L. Zhang, Preparation of $BiVO_4$ by microwave-hydrothermal synthesis and its photocatalytic degradation of ARS under visible light, Technol. Water Treat., 41 (2015) 39–42.
[31] S. Phiankoh, R. Munprom, Effect of pH on crystal structure and morphology of hydrothermally-synthesized $BiVO_4$, Mater. Today Proc., 5 (2019) 9447–9452.
[32] D. Kong, W. Li, T. Yan, Z. Wang, D.S. Kong, J. You, Preparation of novel $BiVO_4$ nanofibers and their excellent adsorptive properties, Mater. Res. Bull., 105 (2018) 84–90.
[33] J. Tian, Q. Shao, J. Zhao, D. Pan, M. Dong, C. Jia, T. Ding, T. Wu, Z. Guo, Microwave solvothermal carboxymethyl chitosan templated synthesis of TiO_2/ZrO_2 composites toward enhanced photocatalytic degradation of Rhodamine B, J. Colloid Interface Sci., 541 (2019) 18–29.
[34] A. Kotta, S.A. Ansari, N. Parveen, H. Fouad, O.Y. Alothman, U. Khaled, H.K. Seo, S.G. Ansari, Z.A. Ansari, Mechanochemical synthesis of melamine doped TiO_2 nanoparticles for dye-sensitized solar cells application, J. Mater. Sci. Mater. Electron., 29 (2018) 9108–9116.
[35] H. Lin, H.T. Zhang, D. Peng, Y. Zhou, Z. Yi, Dynamic behavior of $BiVO_4$ material under mechanical studies, J. Alloys Compd., 774 (2019) 651–655.
[36] X. Tao, L. Shao, R. Wang, H. Xiang, B. Li, Synthesis of $BiVO_4$ nanoflakes decorated with AuPd nanoparticles as selective oxidation photocatalysts, J. Colloid Interface Sci., 541 (2019) 300–311.
[37] S. Ikeda, T. Kawaguchi, Y. Higuchi, N. Kawasaki, T. Harada, M. Remeika, Effects of Zirconium doping into a monoclinic scheelite $BiVO_4$ crystal on its structural, photocatalytic, and photoelectrochemical properties, Front. Chem., 6 (2018) 1–6.
[38] N.P. Moraes, F.N. Silva, M.L.C.P. Silva, T.M.B. Campos, G.P. Thim, L.A. Rodrigues, Methylene blue photodegradation employing hexagonal prism-shaped niobium oxide as heterogeneous catalyst: effect of catalyst dosage, dye concentration, and radiation source, Mater. Chem. Phys., 214 (2018) 95–106.
[39] T. Tikhomirova, G.R. Ramazanova, V.V Apyari, Effect of nature and structure of synthetic anionic food dyes on their sorption onto different sorbents: peculiarities and prospects, Microchem. J., 143 (2018) 305–311.
[40] X. Zhao, J. Hu, S. Chen, Z. Chen, An investigation on the role of W doping in $BiVO_4$ photoanodes used for solar water splitting, Phys. Chem. Chem. Phys., 20 (2018) 13637–13645.

[41] H. Razavi-Khosroshahi, S. Mohammadzadeh, M. Hojamberdiew, S. Kitano, M. Yamauchi, M. Fuji, $BiVO_4$/BiOX (X = F, Cl, Br, I) heterojunctions for degrading organic dye under visible light, Adv. Powder Technol., 30 (2019) 1290–1296.
[42] H. Li, Y. Zhao, C. Yin, L. Jiao, L. Ding, WO_3 nanocrystal prepared by self-assembly of phosphotungstic acid and dopamine for photocatalytic degradation of Congo red, Colloids Surf., A, 572 (2019) 147–151.
[43] S. Aghabeygi, L. Hashemi, A. Morsali, Synthesis, and characterization of ZnO nano-rods via thermal decomposition of Zinc(II) coordination polymers and their photocatalytic properties, J. Inorg. Organomet. Polym., 26 (2016) 495–499.
[44] H. Guo, K. Lin, Z. Zhang, F. Xiao, S. Li, Sulfanilic acid-modified P25 TiO_2 nanoparticles with improved photocatalytic degradation on Congo red under visible light, Dyes Pigm., 92 (2012) 1278–1284.
[45] F.Z. Akika, M. Benamira, H. Lahmar, A. Tibera, R. Chabi, L. Avramova, S. Suzer, M. Trari, Structural and optical properties of Cu-substitution of $NiAl_2O_4$ and their photocatalytic activity towards Congo red under solar light irradiation, J. Photochem. Photobiol., A, 364 (2018) 542–550.
[46] S.K. Kansal, R. Lamba, S.K. Mehta, A. Umar, Photocatalytic degradation of Alizarin red S using simply synthesized ZnO nanoparticles, Mater. Lett., 106 (2013) 385–389.
[47] S. Akshatha, S. Sreenivasa, L. Parashuram, V. Kumar, S.C. Sharma, H. Magalohushana, S. Kumar, T. Maiyalagan, Synergistic effect of hybrid Ce^{3+}/Ce^{4+} doped Bi_2O_3 nano-sphere photocatalyst for enhanced photocatalytic degradation of Alizarin red S dye and its NUV excited photoluminescence studies, Chem. Eng. J., 7 (2019) 103053.
[48] M.L. Souza, P. Corio, Effect of silver nanoparticles on TiO_2-mediated photodegradation of Alizarin red S, Appl. Catal., B, 136–137 (2013) 325–333.
[49] H. Veisi, S. Tatli, M. Haghgoo, A. Amisama, S. Farahmand, S. Hemmati, Immobilization of palladium nanoparticles on thiol-functionalized multi-walled carbon nanotubes with enhanced photocatalytic activity for the degradation of Alizarin red, Polyhedron, 165 (2019) 9–16.
[50] M. Biswas, W. Oh, Synthesis of $BiVO_4$-GO-PVDF nanocomposite: an excellent, newly designed material for high photocatalytic activity towards organic dye degradation by tuning band gap energies, Solid State Sci., 80 (2018) 22–30.
[51] Z. Ye, X. Xiao, J. Chen, Y. Wang, Fabrication of $BiVO_4$/BiOBr composite with enhanced photocatalytic activity by a CTAB-assisted polyol method, J. Photochem. Photobiol., A, 368 (2019) 153–161.
[52] B. Samran, S. Lunput, S. Tonnonchiang, S. Chaiwichian, $BiFeO_3$/$BiVO_4$ nanocomposite photocatalysts with highly enhanced photocatalytic activity for Rhodamine B degradation under visible light irradiation, Physica B, 561 (2019) 23–28.